

Investigation of High-Speed Train Drag with Towing Tank Experiments and CFD

J. Tschepe¹ · D. Fischer² · C. N. Nayeri¹ ·
C. O. Paschereit² · S. Krajnovic³

Received: 17 January 2018 / Accepted: 25 June 2018 / Published online: 24 July 2018
© Springer Nature B.V. 2018

Abstract In order to assess the accuracy of drag prediction methods for high-speed trains, experimental and numerical investigations were performed. Besides the drag coefficient, skin friction and pressure distributions on and near the model have been measured for a 1:22 model of the ICE/V. For the experiments, a moving model rig called DIWA (Drag measurement in water) was realised in a 120 m long towing tank to allow for a realistic simulation of the flow around the train, even in the underbelly region. Numerical investigations were performed using Partially-averaged Navier-Stokes (PANS) simulations based on the k - ω -SST turbulence model. Both experimental and numerical methods can be considered as a novelty in the field of train aerodynamics. The results are compared with data from full-scale tests. It is shown, that the moving model rig DIWA allows for the measurement of drag coefficients of trains with high accuracy. Furthermore, the data acquired using the PANS approach compares well with the experimental data.

Keywords Towing tank · Moving model · Drag measurement · Train aerodynamics · PANS

1 Introduction

The aerodynamic drag of rail vehicles contributes to about 40–70% of the driving resistance, depending on the train shape and velocity [1–3]. Therefore, an accurate prediction

✉ J. Tschepe
tschepe@bit-berlin.de
D. Fischer
d.fischer@tu-berlin.de

¹ Berliner Institut für Technologietransfer (BIT GmbH), Berlin, Germany

² Chair of Fluid Dynamics, Technische Universität Berlin, Berlin, Germany

³ Department of Applied Mechanics, Chalmers University of Technology, Gothenburg, Sweden

of the aerodynamic drag is of high importance for energy demand and optimization [4, 5]. Conventional methods for the determination of aerodynamic drag are either expensive, complicated [6, 7] and not feasible in an early design stage (e.g. full-scale tests) or too oversimplified to represent the complex flow situation around a real train running on track. The latter applies both to conventional wind tunnel tests with short or very small-scale models (typical scales: 1:15 - 1:30) and insufficient ground simulation as well as for numerical simulations with mostly insufficient resolution of turbulence around the vehicle [8–11]. A moving model towing tank facility has been developed in order to provide an experimental method for model scale investigations with realistic boundary conditions, e.g. ground simulation, train length, and Reynolds number, which are the main issues of conventional wind tunnel testing. A static ground is influencing the whole flow field underneath and behind the vehicle and hence, leads to incorrect (in case of train models usually underestimated) drag measurements [8, 9, 12–15]. The boundary layer development and thickness along a train and therefore the flow structures at the rear end of the train, depend highly on the train's length [16–18]. Hence, extrapolations of shortened train configurations to longer variants can only be performed by increasing the boundary layer thickness of downstream cars artificially [19, 20]. This of course requires detailed knowledge of the boundary layer development and can only simulate the real conditions to a certain extent. The influence of Reynolds number effects has already been subject of some studies before [21–24]. From these results it can be assumed, that for Reynolds numbers¹ above about 0.75 Mio. only minor changes in drag measurement will occur. However, the effects seem to be strongly influenced by the respective geometry, therefore the Reynolds number should be as close to the full-scale value as possible [22, 23].

Ground simulation and Reynolds number, as well as the correct development of the flow characteristics along the train are important issues for numerical simulations as well. In order to study the accuracy of a turbulence resolving CFD model, computational investigations using a Partially-averaged Navier-Stokes (PANS) model have been performed. Investigations of Krajnovic et al. using a $k-\epsilon-\zeta$ -f PANS model [25, 26] already showed great potential of the PANS approach for train aerodynamics. Data was compared between both approaches, CFD and towing tank experiments, as well as to full-scale measurement results. Besides drag coefficients, surface pressures, skin friction, and head pressure pulse have been investigated as well to allow for a more detailed comparison.

2 Investigated Train Model

The investigated train model is a 1:22 scale model ($L = 2.99$ m, $H = 0.17$ m) of the 3-car so called *InterCity Experimental* (also known as ICE/V), a prototype of the ICE1 by the Deutsche Bahn. Intensive investigations by Peters [2, 27–29] provide model and full-scale reference data for a 3-, 4- and 5-car train. Two different variants of the train model geometry were considered in the current investigations, in order to quantify the ability of the CFD approach to deal with different levels of geometrical complexity: One variant with simplified bogies and no equipment on the roof and one with detailed bogies and generic roof elements (see Figs. 1 and 2). The pantographs have not been modelled in order to reduce complexity and probable Reynolds number effects. The inter-car gaps are closed, like on the original ICE/V.

¹ $Re = \frac{U \cdot L_{ref}}{\nu}$, $L_{ref} = 3$ m at full-scale

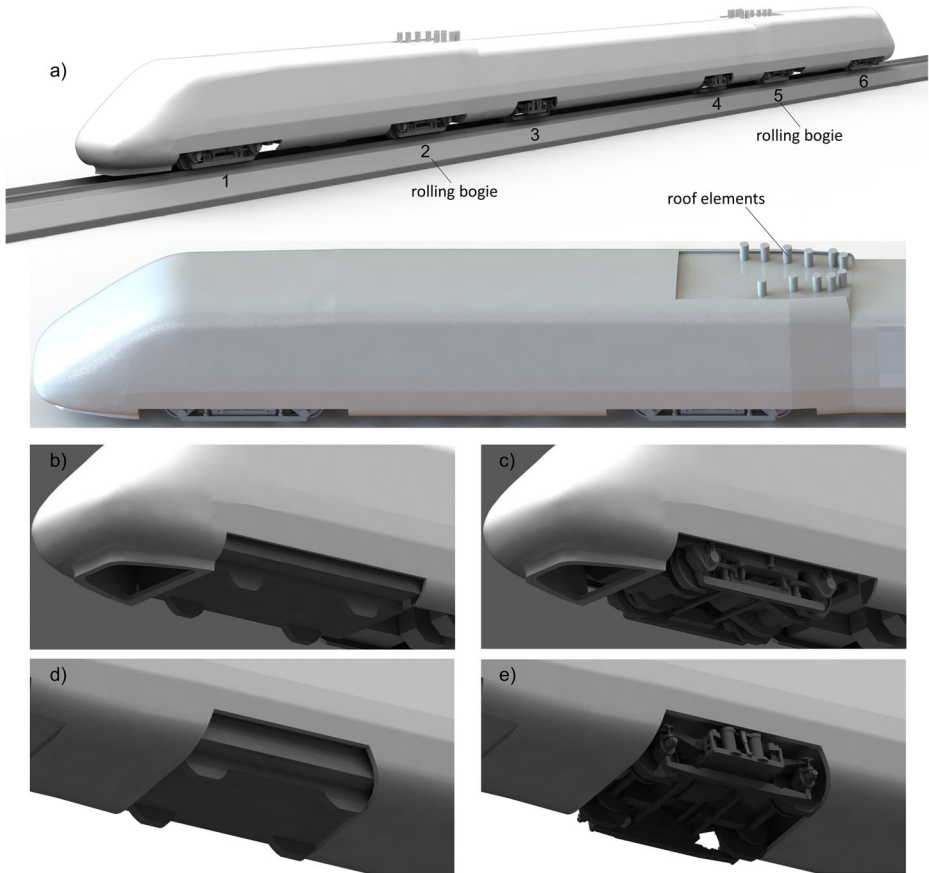


Fig. 1 Investigated train model - **a** train in complex configuration, **b** simple bogies on end cars, **c** complex bogies on end cars, **d** simple bogies on mid car, **e** complex bogies on mid car

For the experiments, only the 2nd and 5th bogie (Fig. 1) were designed as rolling bogies in order to keep the mechanical system simple and reduce rolling resistance. All other bogies had their wheels cut 2 mm above the rails to avoid contact. In the CFD simulations, all



Fig. 2 Model (simple configuration) in empty towing tank

wheels were cut at the same height. In order to generate similar conditions in experiments and simulations, investigations using a tripping tape (Fig. 3) for turbulent transition were conducted.

3 Experimental Setup

Moving model facilities have become a useful tool for aerodynamic investigation of trains as they allow for realistic boundary conditions at model scale [30–34]. However, the use of scaled models requires high velocities to reach Reynolds numbers comparable to the real train. Since the models usually are driven by catapults to reach the required velocity on a suitable track length, strong acceleration forces on the model are inevitable. Devices to prevent the model from derailing are the consequence, leading to mechanical friction that is hard to differentiate from other forces in the acquired data. As the aerodynamic drag of a moving model cannot be determined individually but has to be extracted from the total driving resistance, all forces beside the aerodynamic drag have to be either known or negligibly small. A moving model towing tank setup presents itself as an ideal test configuration for a number of reasons. Due to the physical properties of water, equivalent Reynolds numbers as obtained in air can be achieved at 12–15 times lower speeds in water (Fig. 4). Thus, high accelerations and mechanically complex systems can be avoided. Additionally, at equivalent Reynolds numbers the fluid dynamic forces are four times higher than in air. This leads to a significant change in the power ratio of fluidic to mechanical forces, making the towing tank the most attractive option for drag determination (Fig. 4). In order to transfer the results from water to air and model-scale to full-scale, physical similarity must be complied. For transferability from water to air this especially requires that neither surface waves nor cavitation should affect the results.

The onset of cavitation can be estimated by the incipient cavitation number [35], which is defined as

$$\sigma_i = \frac{p_{amb} - p_{vap}}{q} \quad , \quad (1)$$

with ambient pressure p_{amb} , vapour pressure p_{vap} and dynamic pressure q . If the absolute value of the minimum pressure coefficient exceeds the cavitation number ($|c_{p,min}| \geq \sigma_i$) cavitation might occur. Figure 5 shows the cavitation number for the towing tank tests depending on submergence and towing speed. The incipient cavitation number increases



Fig. 3 First car with (right) and without (left) tripping tape (12 mm × 0.4 mm)

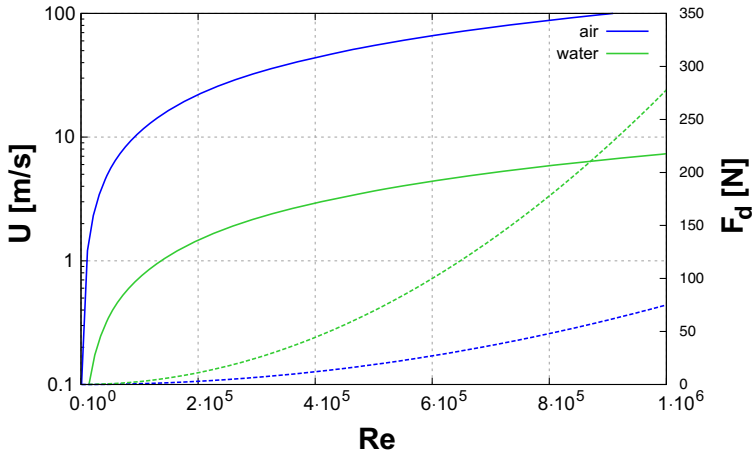


Fig. 4 Velocity U — and drag-force F_d - - - as a function of Reynolds number in air and water (for arbitrary 1:22 model with drag-coefficient $c_d = 0.5$)

with submergence due to a rising hydrostatic pressure level. Assuming that the minimal pressure coefficient for a train is in the range of $c_p = -3$ to -4 , the maximum possible velocity for non-cavitating flow is about $U = 7 - 8$ m/s, which is the equivalent of a Reynolds number of about $Re = 8 - 9 \cdot 10^5$ (reference-length $L_{ref} = 3$ m in full-scale). From the CFD simulations a minimum of $c_p = -1$ was shown to be expectable for the ICE/V, therefore no cavitation should occur at the velocities investigated.

The generation of waves is more difficult to predict, as it depends on the model’s shape, submergence depth and velocity. The resulting resistance depends on wave height and interference patterns. As for ships and submarines, the most unfavourable conditions and hence

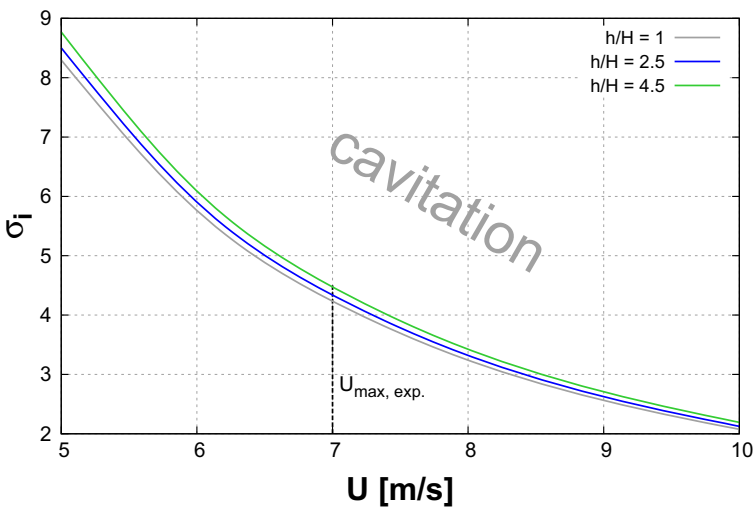


Fig. 5 Cavitation-number as a function of velocity for different depths of water

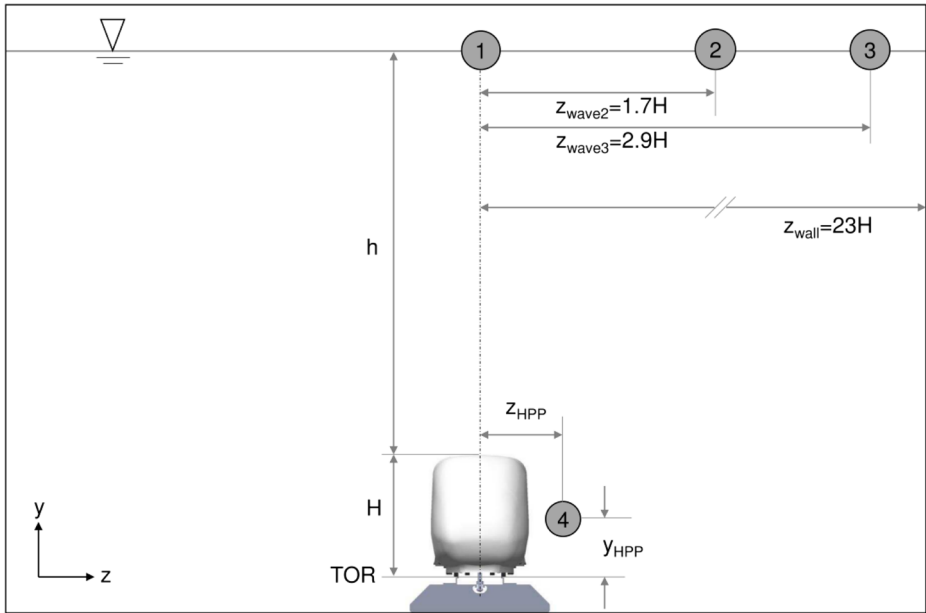


Fig. 6 Experimental setup - position of external sensors (1-3: wave sensors, 4: static pressure probe), $h/H = 2.5$

wave resistance appear at a Froude number² of about $Fr = 0.54$, shifting towards smaller Froude numbers with decreasing depth of water [36]. Below $Fr = 0.3$ and above $Fr = 1.0$ in most cases the wave resistance should become sufficiently small to be neglected, if the submergence depth h/H is at least 2.5 times model height [37–39]. In order to reach high Reynolds numbers, only $Fr \geq 1.0$ is of interest for train model investigations. For the model investigated in this paper $Fr = 1$ is reached at around $U = 5.5$ m/s. Hence, it can be concluded that towing tank tests with train models should be performed at a submergence of at least 2.5 times model height and within a velocity range of 5 – 8 m/s to avoid both influences of cavitation and wave resistance.

The current investigations were performed at three different submergence depths ($h/H = 1, 2.5, 4.5$) and a velocity range of $U = 3 - 7$ m/s ($3.5 \cdot 10^5 \leq Re \leq 8.5 \cdot 10^5$) in order to investigate the influence of waves on the drag measurement (due to an insufficient range of the pressure sensor for the highest velocity, the skin friction has been investigated at $U = 1 - 6$ m/s). The wave height was measured by wave sensors at different positions. A stationary Pitot tube was used to measure the head pressure pulse at $z_{HPP} = 2.5$ m (full-scale values) beside the centre of track and $y_{HPP} = 1.8$ m above top of rail (Fig. 6). The model itself was equipped with pressure sensors³ for measurement of static pressure on the train head and tail, Preston tubes for skin friction measurements, acceleration sensors and a force sensor⁴ for drag determination. The towing mechanism was placed inside the track and directly attached to the force sensor inside the model (Fig. 7). All data was stored by a

² $Fr = \frac{U}{\sqrt{gL}}$, L: length of train model

³Honeywell differential pressure sensor 26PC series (range: 7 & 35 kPa, resolution: 0.5%)

⁴HBM S9M (range: ± 2 kN, resolution: 0.01%)

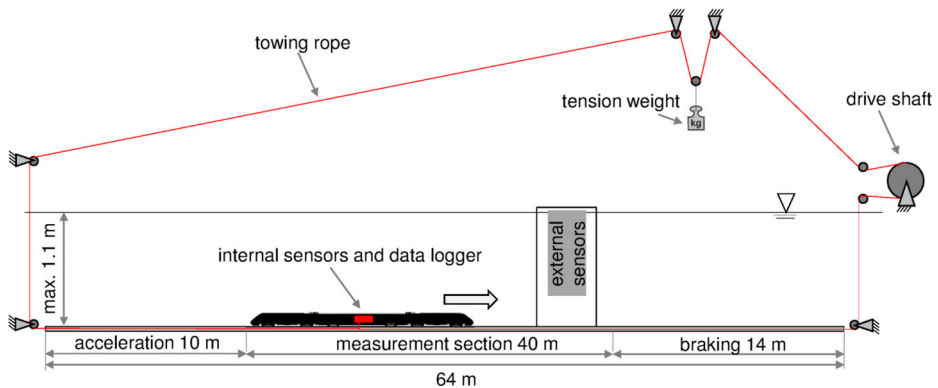


Fig. 7 Experimental setup - towing tank

data logger inside the model. Frequency measurement of the towing motor, light gates along the track and acceleration sensors inside the model allowed for a precise determination of the time resolved model velocity.⁵

4 Numerical Setup

The CFD simulations were conducted using the open-source framework *OpenFOAM*. The experimental setup was simulated including ballast, rails, moving ground and the respective train models without further simplifications. To the knowledge of the authors, the simulations constitute a first attempt to use *OpenFOAM* in conjunction with PANS methods for the aerodynamic simulation of trains.

The extend of the CFD domain and train position are presented in Fig. 8. Unstructured, hexahedral meshes consisting of about 13M (simple) and 19M cells (complex) were used, generated by the *OpenFOAM* meshing tool *snappyHexMesh*. The mesh features predominantly cubic cells and multiple refinement regions, with special regard to the flow underneath the train, at the train roof and the wake, with a resolution of $0.5 \cdot 10^{-3}L$ close to the surface and $1 \cdot 10^{-3}L$ in the wake and underbelly region. The near-wall flow was resolved by 10 prism layers with a growth rate of 1.15, which allowed a wall-normal distance for the majority of cells of $y^+ = [25, 50]$. Hence, wall-functions based on the $k - \omega - SST$ wall-functions implemented in *OpenFOAM* were used to model the near-wall behaviour of turbulence. Note that the use of the high-Reynolds approach here is just a first attempt to apply the implemented PANS model to such a complex geometry. The simulations will be followed by low-Reynolds simulations on an adequate mesh with fully resolved boundary layer.

Simulations were conducted for $Re = 8.2 \cdot 10^5$. Sides and top of the domain were modelled as free-stream surfaces while the ground, ballast and rails were modelled as no-slip moving walls. The pressure was fixed at the outlet, while a constant velocity was prescribed on the inlet. A turbulence intensity of 1% was assumed at the inlet to match the experiment.

The incompressible, transient solver *pimpleFoam* was used. Convective fluxes were approximated using second-order, upwind-biased bounded central differences, while a

⁵resolution: 0.7%

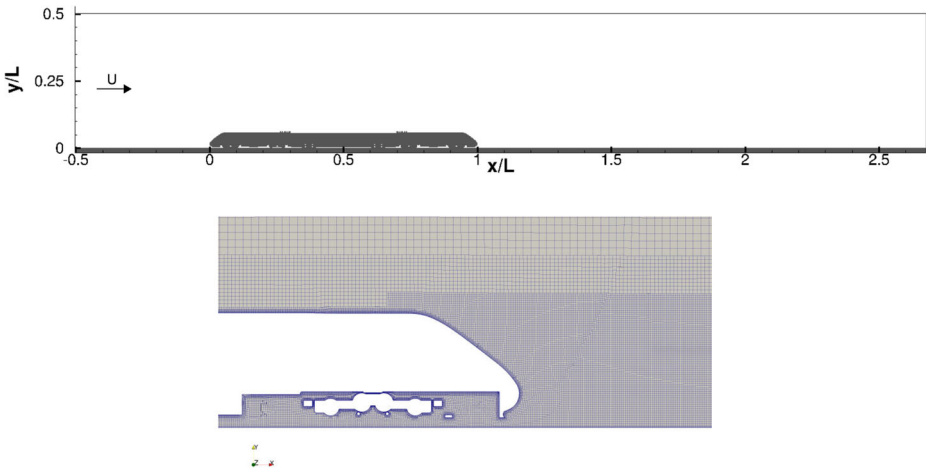


Fig. 8 CFD Domain, $z/L = [-0.25, 0.25]$ and slice through mesh

second-order accurate implicit scheme was used for time discretisation. A time step of $\Delta t = 0.00017 \frac{H}{u_{in}}$ was chosen to ensure $CFL < 1$ for nearly all cells. The simulations were initialised with a stationary RANS simulation, followed by 90 CTU⁶ initial transient PANS simulation. The flow field was averaged over another 175 CTU.

Turbulence is modelled using the Partially-averaged Navier-Stokes approach [40]. A $k-\omega$ -SST PANS model based on the works of Lakshmipathy et al. [41, 42] was implemented in *OpenFOAM*. The approach utilises the unresolved-to-total ratios of turbulent kinetic energy f_k and dissipation f_ϵ to control the amount of averaging and blend between the underlying RANS model ($f_k = 1$) and DNS ($f_k = 0$). For high Reynolds numbers $f_\epsilon = 1$ can be assumed.

$$f_k = \frac{k_u}{k} = \frac{k_u}{k_u + k_r} \tag{2}$$

$$f_\omega = \frac{f_\epsilon}{f_k} \tag{3}$$

A detailed derivation and description of the PANS concepts can be found in [40]. In the implemented $k-\omega$ -SST PANS model, transport equations are solved for the unresolved turbulent kinetic energy k_u and unresolved specific dissipation rate ω_u . All model parameters were kept at their standard values for the $k-\omega$ -SST model.

$$\frac{\partial k_u}{\partial t} + \frac{\partial u_i k_u}{\partial x_i} = P_u - \beta^* k_u \omega_u + \frac{\partial}{\partial x_i} \left[(v + \sigma_{ku} \nu_t) \frac{\partial k_u}{\partial x_i} \right] \tag{4}$$

$$\frac{\partial \omega_u}{\partial t} + \frac{\partial u_i \omega_u}{\partial x_i} = P_u \gamma \left(\frac{\omega_u}{k_u} \right) - \beta' \omega_u^2 + \frac{\partial}{\partial x_i} \left[(v + \sigma_{\omega u} \nu_t) \frac{\partial \omega_u}{\partial x_i} \right] + 2(1 - F_1) \frac{\sigma_{\omega 2u}}{\omega_u} \frac{\partial k_u}{\partial x_i} \frac{\partial \omega_u}{\partial x_i} \tag{5}$$

$$P_u = \nu_t \frac{\partial u_i}{\partial x_j} \left[\frac{\partial u_i}{\partial x_j} + \frac{\partial u_j}{\partial x_i} \right] \tag{6}$$

$$\sigma_{ku} = \sigma_k \frac{f_\omega}{f_k}, \quad \sigma_{\omega u} = \sigma_\omega \frac{f_\omega}{f_k} \tag{7}$$

⁶CTU = $t \cdot \frac{U_{in}}{H}$, U_{in} : free-stream velocity

$$\beta' = \gamma\beta^* - \frac{\gamma\beta^*}{f_\omega} + \frac{\beta}{f_\omega} \tag{8}$$

Furthermore, f_k was used as time-dependant parameter, depending on local grid size Δ and turbulence length scale Λ , which is predicted at the end of every time step and used as constant in the next one. Foroutan [43] derived an improved formula for f_k , which was used here:

$$f_k = 1 - \left[\frac{\left(\frac{\Lambda}{\Delta}\right)^{\frac{2}{3}}}{0} .23 + \left(\frac{\Lambda}{\Delta}\right)^{\frac{2}{3}} \right]^{4.5} \tag{9}$$

$$\Lambda = \frac{k^{\frac{2}{3}}}{\epsilon} = \frac{\sqrt{k}}{\beta^*\omega}, \quad \Delta = (\Delta_x \Delta_y \Delta_z)^{\frac{1}{3}} \tag{10}$$

To avoid the problems associated with averaging to acquire the turbulent length scale Λ at each time step, an additional transport equation for the scale-supplying variable k_{SSV} is solved as suggested by Basara et al. [44]:

$$f_k = \frac{k_u}{k} = \frac{k_u}{k_u + k_{SSV}} \tag{11}$$

$$\frac{\partial k_{SSV}}{\partial t} + \frac{\partial u_i k_{SSV}}{\partial x_i} = \frac{k_{SSV}}{k_u} (P_u - \beta^* k_u \omega_u) + \frac{\partial}{\partial x_i} \left[(v + \sigma_{ku} \nu_t) \frac{\partial k_{SSV}}{\partial x_i} \right] \tag{12}$$

Initial validations on generic bluff bodies showed good agreement to DDES data and improved performance compared to RANS simulations, especially for drag prediction of more complex geometries [45].

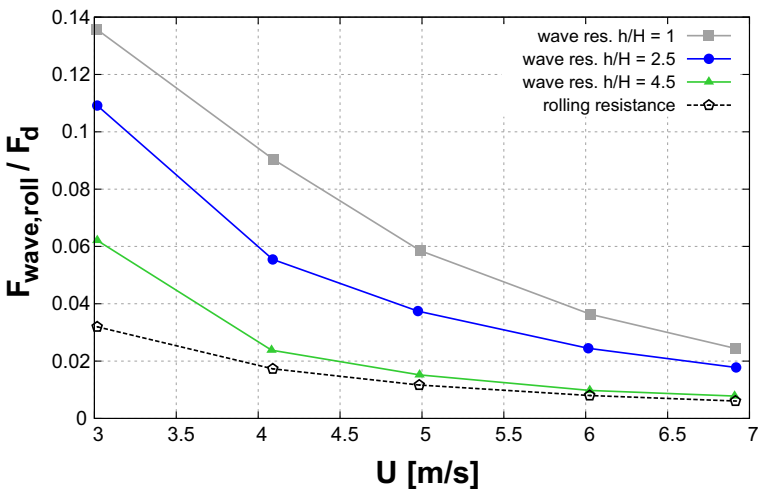


Fig. 9 Influence of wave and rolling resistance on drag-force over velocity - experiments

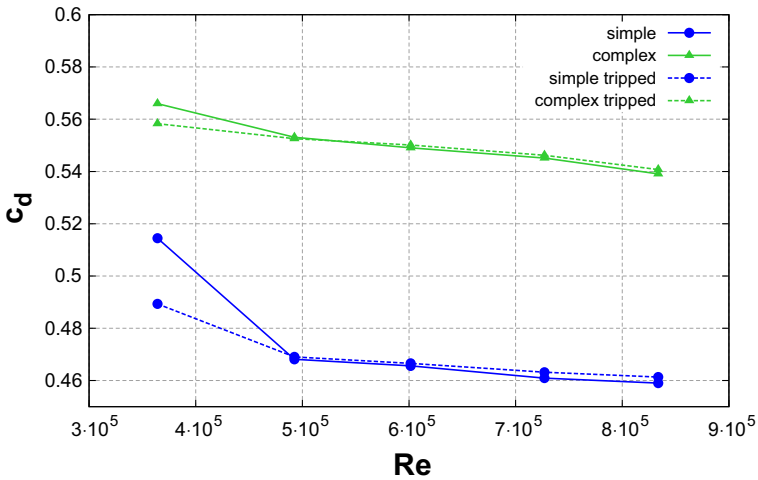


Fig. 10 Drag coefficient as a function of Reynolds number - experiments

5 Results

The drag coefficient⁷ from the towing tests was determined by subtracting the rolling resistance and wave resistance from the measured running resistance. The average of three measurement runs was taken for each Reynolds number at a constant velocity over an averaging period of about 4 seconds. While the wave resistance was calculated from the measured water level along the model, i.e. the hydrodynamic pressure difference at head and tail [46], the rolling resistance was determined with a measurement at very low speed ($U \approx 0.15$ m/s). As shown in Fig. 9, for the highest velocities at deepest submergence rolling and wave resistance each contribute less than 1% to the running resistance. Hence, uncertainties regarding their precise determination are of less importance than for moving model facilities operating in air, where the mechanical resistance contributes about 30% of the total resistance [33]. However, for lower velocities a consideration of all resistance parts becomes necessary to determine the correct amount of drag.

The drag coefficients extracted from the experiments, both with and without the tripping tape on the first car, are shown for different Reynolds numbers in Fig. 10. Only a slight decrease of the drag coefficient can be observed for both configurations for $Re > 5 \cdot 10^5$, showing marginally higher values with the tripping tape applied. However, these deviations are well within measurement precision ($\pm 1\%$). At lower Reynolds numbers, the drag seems to change more drastically. The high drag coefficient at the lowest Reynolds number presented in Fig. 10 is most likely a result of uncertainties in the calculated wave resistance (Fig. 9). Furthermore, without tripping tape and at lower Reynolds numbers the flow around the model may not be considered fully turbulent [23], which especially affects the skin friction at the model’s surface. Hence, the high amount of frictional drag (see Table 1) and its

⁷ $c_d = \frac{F_d}{\frac{\rho}{2} U^2 A_{ref}}$, $A_{ref} = 10 \text{ m}^2$ (full-scale)

Table 1 Skin friction coefficient c_f integrated over train surface A_{train} (excluding bogies) at $Re = 8.2 \cdot 10^5$ and estimate by Peters for the full-scale train [27, 28]; frictional drag coefficient $c_{d,f} = (c_f \cdot A_{train})/A_{ref}$

	$\int c_f dA_{train}$	$c_{d,f}$	$c_{d,f} / c_d$
Peters	0.002	0.1677	0.335
CFD (simple)	0.0022	0.1670	0.377
CFD (complex)	0.0024	0.2012	0.379

distinct Reynolds number dependency (Fig. 11) require high Reynolds numbers for accurate drag determination of high-speed trains. From the skin friction coefficient given for the full-scale data (see Table 1) it can be assumed that the skin friction coefficient at the highest Reynolds number investigated nearly reached turbulent saturation and is not supposed to further drop significantly. Hence, similar behaviour can be assumed for the drag coefficient.

From here on, all results presented are from experiments and CFD simulations with $Re = 8.2 \cdot 10^5$. Table 2 and Fig. 12 show the drag coefficient determined by the experiments and CFD calculations compared to the full-scale value given by Peters [2]. It can be seen that experimental and numerical data are very close to each other, with about 3% smaller values for CFD. Furthermore, results for the complex variant compare well with the full-scale data. Here it must be taken into account, that the generic elements on the roof slightly exaggerate the drag generated by the real roof elements and pantograph. This is due to the fact that they were designed to represent the drag of roof equipment and lifted pantograph but were placed on first and last car [47]. However, the real three-car train has been investigated with only one pantograph lifted, generating slightly less aerodynamic drag. This assumption is supported by the drag contribution of the single cars, as shown in Fig. 13. The drag coefficient of the complex middle car, which has no roof elements, is very close to the one given by Peters [2, 27]. The drag observed for the complex first and last car shows a higher drag coefficient than determined by Peters. This is most probably due to the simplified generic roof elements [47]. A comparison between the simple and complex variant shows that the drag of the complex variant appears to be more equally distributed. This can be

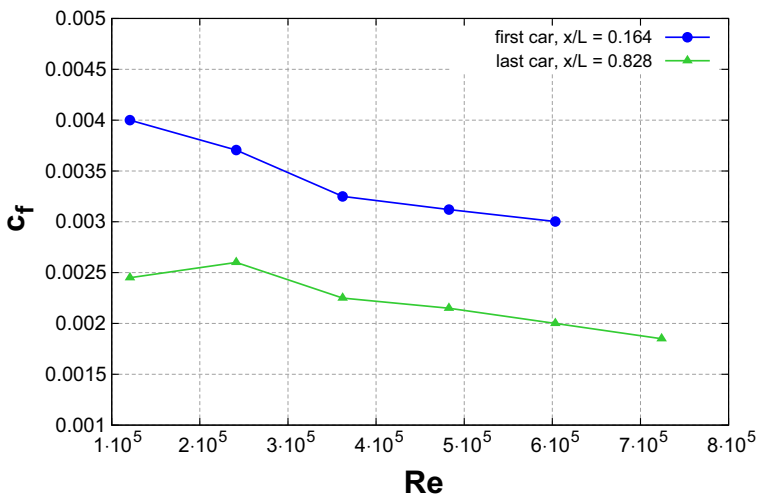


Fig. 11 Skin friction coefficient as a function of Reynolds number for complex configuration without tripping tape, measured on train roof - experiments

Table 2 Drag coefficient c_d for different model configurations at $Re = 8.2 \cdot 10^5$, full-scale measurements at $Re = 5 - 16 \cdot 10^6$ (coasting tests)

	c_d	Δc_d
Full-scale	0.500	–
Experiment (simple)	0.458	–8%
CFD (simple)	0.443	–11%
Experiment (complex)	0.539	+8%
CFD (complex)	0.531	+6%

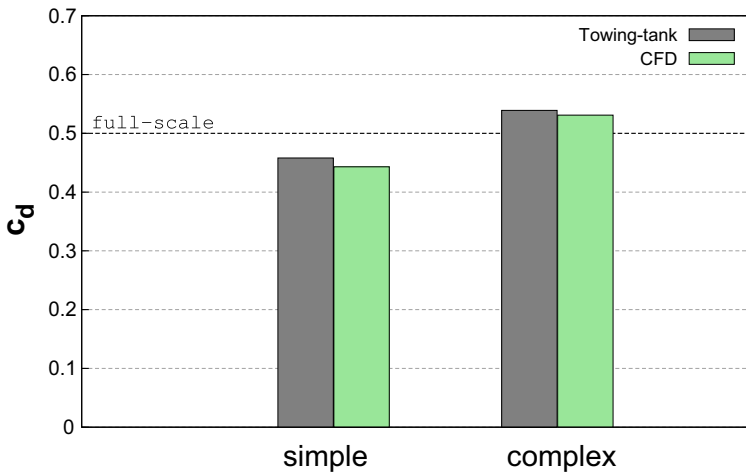


Fig. 12 Drag coefficient for different model configurations, $Re = 8.2 \cdot 10^5$

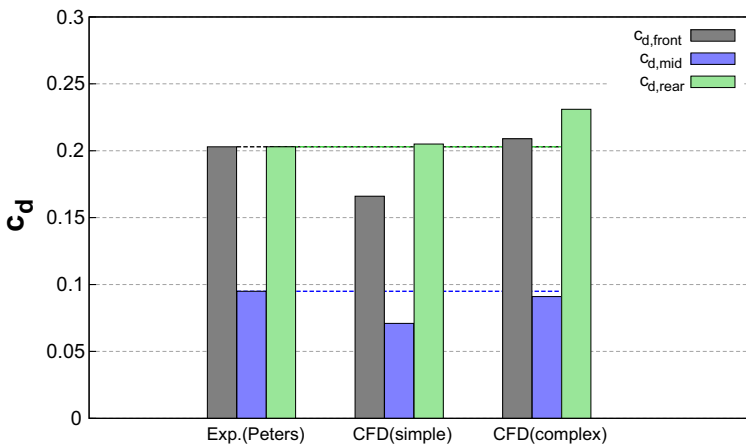


Fig. 13 Drag contribution by cars

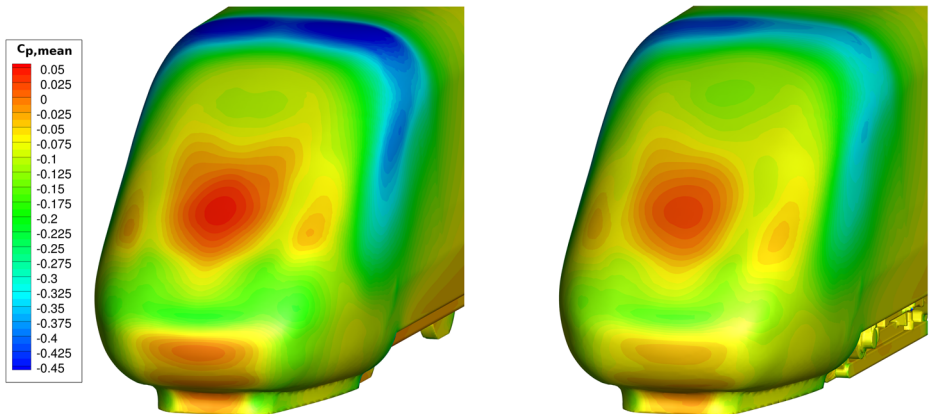


Fig. 14 Pressure distribution on trailing car - CFD (left: simple, right: complex)

explained with the increased drag generated by the bogies of each car and the additional roof elements, which lead to a stronger drag increase on the front than on the rear car, due to the thinner boundary layer on the leading car.

The high drag contribution of the last car results from the distinct low-pressure regions at the tail (Fig. 14), induced by the vortices typically appearing on hatchbacks [48]. When integrating the pressure over the surface of just the train tail ($x/L > 0.95$), the pressure drag generated here is about 10% lower for the complex variant, indicating a possible positive influence of the altered structure of the stream-wise vortices forming on the train roof (due to the roof elements) in this particular area. The apparent impact of the roof elements on the pressure loss of the trailing car might be another reason for the differences to the results

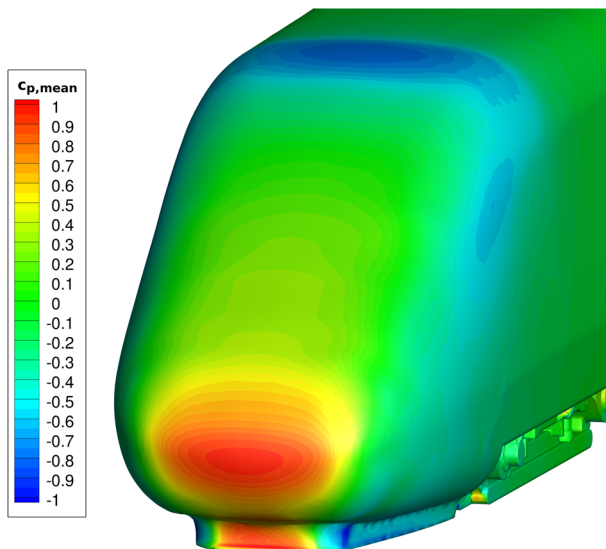


Fig. 15 Pressure distribution on train head - CFD

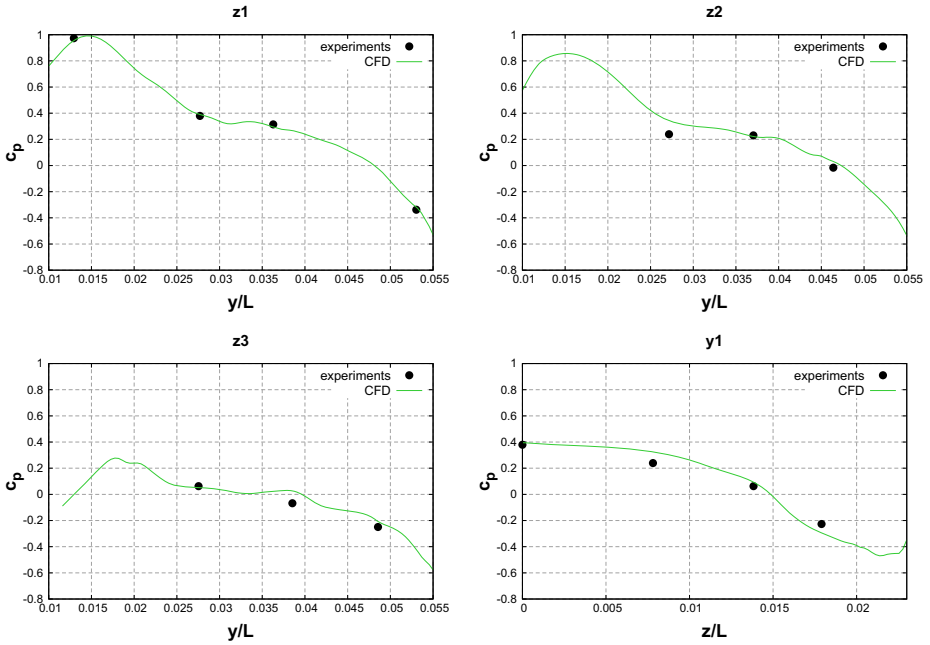


Fig. 16 Pressure coefficient on different slices - head (slice locations shown in Fig. 18)

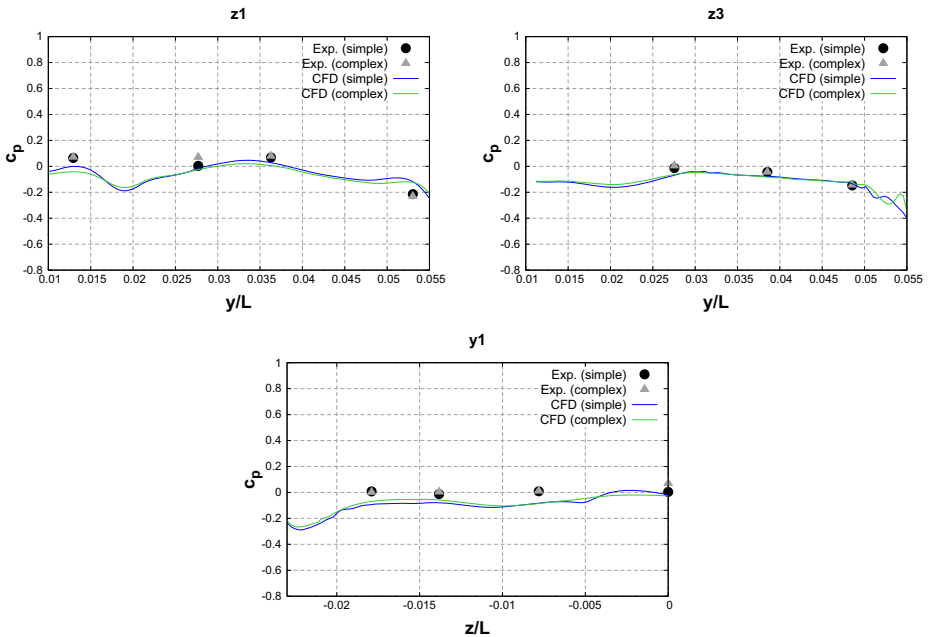


Fig. 17 Pressure coefficient on different slices - tail (slice locations shown in Fig. 18)

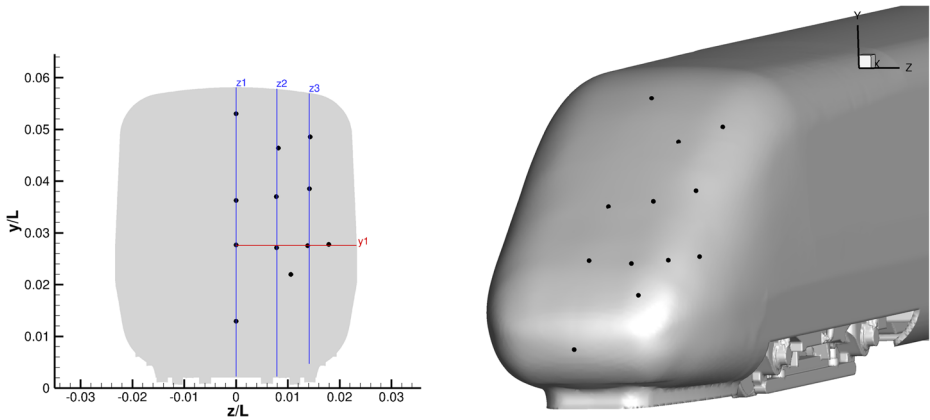


Fig. 18 Position of wall pressure taps on train head/ tail

given by Peters, as an actual Pantograph is supposed to have a different effect on the flow structures downstream.

The pressure distribution on the train head and tail is shown in Figs. 14, 15, 16 and 17. The measurement positions for the experiments can be found in Fig. 18. It can be seen that on both head and tail the agreement between experimental data and simulations is quite good. For the complex variant, the pressure distribution on the rear end appears to be affected by the presence of the asymmetrically distributed roof elements (see Fig. 1) and the flow development downstream of them.

Finally, the head pressure pulse at $y_{HPP} = 1.8$ m and $z_{HPP} = 2.5$ m (full-scale values according to EN14067-4 [49]) is compared for the different geometry variants and methods (Fig. 19). It can be seen, that the results from experiment and CFD compare well qualitatively. However, due to the high forces in the towing tank the static pressure probe was vibrating slightly, affecting the measurement results. An analysis of the probe’s

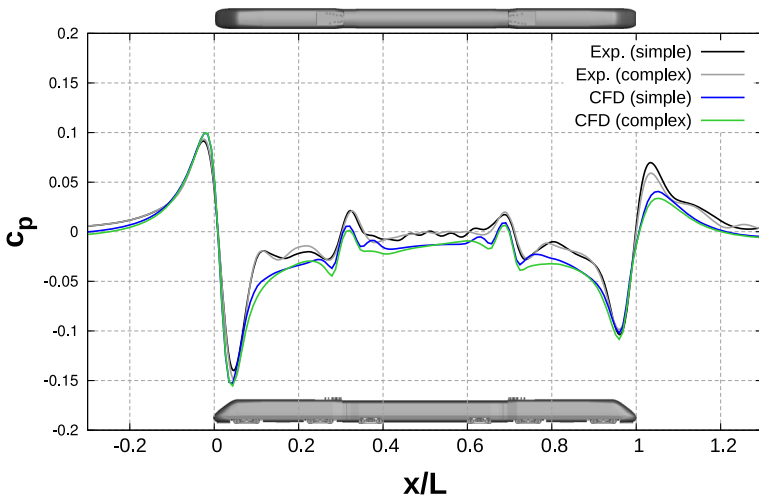


Fig. 19 Head-pressure-pulse at $y/H = 0.48$, $z/W = 0.81$

eigenfrequency allowed to filter⁸ the effect to a certain degree, but some oscillations remain noticeable behind the suction peak at the model's head, continuing along the whole train passage. This makes a deeper comparison somewhat difficult. Nevertheless, the general development of the pressure coefficient along the train agrees well. The head pressure pulse and the pressure variation at the cross-section change along the middle car is quite similar. The differences at the tail's pressure peak are in the same order of magnitude as the differences obtained by the surface pressure measurements on the trailing car, indicating some uncertainties in the numerical simulations. However, due to the aforementioned measurement difficulties, further investigations and counter measures for improved pressure measurement in the towing tank are necessary for a more detailed comparison.

6 Conclusion and Future Work

Submerged moving model experiments as well as Partially-averaged Navier-Stokes simulations were conducted to investigate their prediction accuracy concerning the aerodynamic drag of high-speed trains. In order to get a better insight into the flow characteristics of the model, skin friction and pressure measurements have been performed as well. The comparison of the data acquired by experiments, simulations and full-scale tests showed very convincing results. Both methods seem to be suitable for drag investigations of high-speed trains and evaluation of the flow patterns around them. In order to expand the use of both methods to different vehicle geometries, e.g. freight trains, further investigations are necessary. For the experimental setup, the impact of waves generated by less streamlined and much longer vehicles needs to be investigated. Nevertheless, it can already be stated that the shortcomings of moving model facilities operating in air concerning drag measurement can be overcome by the use of a towing tank setup. For the numerical setup, simulations with improved boundary layer resolution will be subject to further investigations. The $k-\omega$ -SST PANS model in *OpenFOAM* is still subject to validation, hence a detailed comparison with other turbulence models will be conducted. Eventually, simulations at Reynolds numbers closer to those of the full-scale train will be of special interest. Both methods provide different advantages. While the towing tank allows for investigation of a larger amount of configurations and Reynolds numbers within a short time, the CFD provides insight in the whole flow field around the model. Hence, a further development and combined use of both methods appears to be very promising for the assessment and optimization of train aerodynamic drag, as well as the investigation of transient flow effects around trains.

Acknowledgements The experimental research presented was supported by the ZIM program and the BIT GmbH. The project was funded under grant number EP 141376 from the “Zentrales Innovationsprogramm Mittelstand (ZIM)” of the Federal Ministry of Economy and Energy, following a decision of the German Bundestag.

The simulations were performed with resources provided by the North-German Supercomputing Alliance (HLRN).

Compliance with Ethical Standards

Conflict of interests The authors declare that they have no conflict of interest.

⁸3rd-order Butterworth filter, cut-off frequency 30 Hz

Publisher's Note Springer Nature remains neutral with regard to jurisdictional claims in published maps and institutional affiliations.

References

- Nolte, R., Würtenberger, F.: Evaluation of Energy Efficiency Technologies for Rolling Stock and Train Operation of Railways. UIC, Berlin (2003)
- Peters, J.-L.: Bestimmung des aerodynamischen Widerstandes des ICE/v im Tunnel und auf offener Strecke durch Auslaufversuche. Eisenbahntechnische Rundschau **39**(9), 559–564 (1990)
- Lukaszewicz, P.: Running resistance - results and analysis of full-scale tests with passenger and freight trains in Sweden. J. Rail Rapid Transit **221**(2), 183–193 (2007)
- Orellano, A., Kirchhof, R.: Optimising the aerodynamics of high speed trains. Railw. Gaz. Int. **5**, 41–45 (2011)
- Steuger, M.: Velaro - kundenorientierte Weiterentwicklung eines Hochgeschwindigkeitszuges. ZEVrail **133**(10), 414–425 (2009)
- Somaschini, C., Rocchi, D., Tomasini, G., Schito, P.: Simplified Estimation of Train Resistance Parameters: Full Scale Experimental Tests and Analysis. In: the Third International Conference on Railway Technology: Research, Development and Maintenance, Stirlingshire, UK (2016)
- Boschetti, G., Mariscotti, A.: The Parameters of Motion Mechanical Equations as a Source of Uncertainty for Traction System Simulation. In: Proceedings of the IMEKO World Congress, Busan, Korea (2012)
- Kwon, H., Park, Y., Lee, D., Kim, M.: Wind tunnel experiments on Korean high-speed trains using various ground simulation techniques. J. Wind Eng. Ind. Aerodyn. **89**, 1179–1195 (2001)
- Gaylard, A., Howlett, A., Harrison, D.: Assessing Drag Reduction Measures for High-Speed Trains. In: Proceedings of the Vehicle Aerodynamics Conference of the Royal Aeronautical Society, Loughborough, UK (1994)
- Baker, C.: A review of train aerodynamics Part 1 - fundamentals. Aeronautical J. **118**(1201), 201–228 (2014)
- Baker, C.: A review of train aerodynamics Part 2 - applications. Aeronautical J. **118**(1202), 345–382 (2014)
- Zhang, J., Li, J., Tian, H., Gao, G., Sheridan, J.: Impact of ground and wheel boundary conditions on numerical simulation of the high-speed train aerodynamic performance. J. Fluid Struct. **61**, 249–261 (2016)
- Wang, S., Burton, D., Herbst, A., Sheridan, J., Thompson, M.: The effect of the ground condition on high-speed train slipstream. J. Wind Eng. Ind. Aerodyn. **172**, 230–243 (2018)
- Lajos, T.: Effect of moving ground simulations on the flow past bus models. J. Wind Eng. Ind. Aerodyn. **22**, 271–271 (1986)
- Fago, B., Lindner, H., Mahrenholtz, O.: The effect of ground simulation on the flow around the vehicles in wind tunnel testing. J. Wind Eng. Ind. Aerodyn. **38**, 47–57 (1991)
- Jia, L., Zhou, D., Niu, J.: Numerical calculation of boundary layers and wake characteristics of high-speed trains with different lengths. PLoS ONE **12**(12), e0189798 (2017). <https://doi.org/10.1371/journal.pone.0189798>
- Muld, T., Efraimsson, G., Hennigson, D.S.: Wake characteristics of high-speed trains with different lengths. J. Rail Rapid Transit, Proc. Inst. Mech. Eng. Part F. **228**(4), 333–342 (2013)
- Bell, J.R., Burton, D., Thompson, M.C., Herbst, A.H., Sheridan, J.: A wind-tunnel methodology for assessing the slipstream of high-speed trains, Journal of Wind Engineering and Industrial Aerodynamics, vol. 166 published online (2017)
- Neppert, H.: Komponenten-widerstände im Einfluss der Grenzschicht an zügen variable länge. ZEV-Glasers Annalen **108**(9), 239–247 (1984)
- Ido, A.: Energy-saving in conventional trains by aerodynamic drag reduction. Japanese Railway Eng. **188**, 2–4 (2015)
- Baker, C.J., Brockie, N.J.: Wind tunnel tests to obtain train aerodynamic drag coefficients: Reynolds number and ground simulation effects. J. Wind Eng. Industrial Aerodynamics **38**, 23–28 (1991)
- Peters, J.-L.: Effect of Reynolds number on the aerodynamic forces on a container model. J. Wind Eng. Ind. Aerodyn. **49**, 431–438 (1993)
- Willemsen, E.: High Reynolds number wind tunnel experiments on trains. J. Wind Eng. Ind. Aerodyn. **69-71**, 437–447 (1997)

24. Niu, J., Liang, X., Zhou, D.: Experimental study on the effect of Reynolds number on aerodynamic performance of high-speed train with and without yaw angle. *J. Wind Eng. Ind. Aerodyn.* **157**, 36–46 (2016)
25. Krajnovic, S., Minelli, G.: Status of PANS for bluff body aerodynamics of engineering relevance, progress in hybrid RANS-LES modelling, Texas, USA, 399–410 (2015)
26. Krajnovic, S., Minelli, G.: Partially-averaged Navier-Stokes simulation of the flow around simplified vehicle. In: AIP Conference Proceedings, vol. 1648 (2015)
27. Peters, J.-L.: Luftwiderstand von schnellen Triebzügen bei stationärer Anströmung. In: CCG-Lehrgang V5.02 (1983)
28. Peters, J.-L.: Aerodynamics of very high speed trains and maglev vehicles: state of the art and future potential. *Int. J. Vehicle Des.* **SP3**, 308–341 (1983)
29. Peters, J.-L.: Measurement of the influence of tunnel length on the tunnel drag of the ICE/v train. *Aerodynamics and Ventilation of Vehicle Tunnels*, 739–756 (1991)
30. Sterling, M., Baker, C., Jordan, S., Johnson, T.: A study of the slipstream of high-speed passenger trains and freight trains. *Proc. Instit. Mech. Eng. Part F: J. Rail Rapid Transit* **222**, 177–193 (2008)
31. Baker, C., Dalley, S., Johnson, T., Quinn, A., Wright, N.: The slipstream and wake of a high-speed train. *Proc. Instit. Mech. Eng. Part F: J. Rail Rapid Transit* **215**, 83–99 (2001)
32. Bell, J., Burton, D., Thompson, M., Herbst, A., Sheridan, J.: Moving model analysis of the slipstream and wake of a high-speed train. *J. Wind Eng. Ind. Aerodyn.* **136**, 127–137 (2015)
33. Yang, M., Du, J., Li, Z., Huang, S., Zhou, D.: Moving model test of high-speed train aerodynamic drag based on stagnation pressure measurements. *PLoS ONE*, 1–15 (2017)
34. Yang, Q., Song, J.-H., Yang, G.: A moving model rig with a scale ratio of 1/8 for high speed train aerodynamics. *J. Wind Eng. Ind. Aerodyn.* **152**, 50–58 (2016)
35. Hoerner, S.: *Fluid-Dynamic Drag*, pp. 10–5. CA: Hoerner Fluid Dynamics, Bakersfield (1965)
36. Molland, A., Turnock, S., Hudson, D.: *Ship Resistance and Propulsion: Practical Estimation of Ship Propulsive Power*, pp. 97–107. Cambridge University Press, Cambridge (2011)
37. Gertler, M.: *Resistance Experiments on a Systematic Series of Streamlined Bodies of Revolution*. Navy Department: The David W. Taylor Model Basin, Washington D.C. (1950)
38. Weinblum, G., Amtsberg, H., Bock, W.: *Tests on Wave Resistance of Immersed Bodies of Revolution*. Navy Department: The David W. Taylor Model Basin, Washington D.C. (1950)
39. Wigley, W.: Water forces on submerged bodies in motion. *Trans. Instit. Naval Architects* **95**, 268–279 (1953)
40. Grimajaj, S., Abdol-Hamid, K.: Partially-averaged navier stokes model for turbulence: Implementation and validation. In: 43rd AIAA Aerospace Sciences Meeting and Exhibit (2005)
41. Lakshminpathy, S., Girimaji, S.S.: Partially-averaged navier-stokes method for turbulent flows: k- ω model implementation. AIAA paper, 119 (2006)
42. Lakshminpathy, S., Togiti, V.: Assessment of alternative formulations for the specific-dissipation rate in rans and variable-resolution turbulence models. In: 20th AIAA Computational Fluid Dynamics Conference, p. 3978 (2011)
43. Foroutan, H., Yavuzkurt, S.: A partially-averaged Navier-Stokes model for the simulation of turbulent swirling flow with vortex breakdown. *Int. J. Heat Fluid Flow* **500**, 402–416 (2014)
44. Basara, B., Girimaji, S.: Modelling of the cut-off scale supplying variable in bridging methods for turbulence flow simulation. In: Proceedings of International Conference on Jets, Wakes, and Separated Flows, Nagoya, Japan, pp. 17–21 (2013)
45. Fischer, D., Tschepe, J., Nayeri, C.N., Paschereit, C.O.: Partially-averaged Navier-Stokes method for train aerodynamics. In: Proceedings of the 3rd International Symposium Rail aerodynamics and Train Design (2018)
46. Tschepe, J., Fischer, D., Nayeri, C.N., Paschereit, C.O.: Aerodynamic Drag Measurement of Rail Vehicles by Means of Towing Tank Tests. In: Proceedings of the 3rd International Symposium Rail Aerodynamics and Train Design (2018)
47. Tschepe, J., Nayeri, C.: Untersuchungen zum strömungswiderstand von Schienenfahrzeugen mit bewegten Modellen im Wasserschleppkanal. *ZEV Rail* **142**(4), 124–131 (2018)
48. Östth, J., Kaiser, E., Krajnovic, S., Noack, B.: Cluster-based reduced-order modelling of the flow in the wake of a high speed train. *J. Wind Eng. Ind. Aerodyn.* **145**, 327–338 (2015)
49. EN14067-4 Railway applications - Aerodynamics - Part 4: Requirements and test procedures for aerodynamics on open track (2013)